Received: 10 December 2019 | Revised: 5 February 2020 | Accepted: 4 March 2020

DOI: 10.1002/asl.968

Atmospheric Science Letters RMetS

RESEARCH ARTICLE

The predictability limit of the amplitude and phase of the Madden-Julian oscillation

Deyu Lu[1] | **Ruiqiang Ding**[2] | **Jianping Li**[3]

[1]State Key Laboratory of Numerical Modeling for Atmospheric Sciences and Geophysical Fluid Dynamics (LASG), Institute of Atmospheric Physics, Chinese Academy of Sciences, Beijing, China

[2]State Key Laboratory of Earth Surface Processes and Resource Ecology, Beijing Normal University, Beijing, China

[3]Key Laboratory of Physical Oceanography-Institute for Advanced Ocean Studies, Ocean University of China and Qingdao National Laboratory for Marine Science and Technology, Qingdao, China

Correspondence
Ruiqiang Ding, State Key Laboratory of Earth Surface Processes and Resource Ecology, Beijing Normal University, Beijing, China.
Email: drq@mail.iap.ac.cn

Funding information
The National Key Research and Development Project, Grant/Award Number: 2018YFC1505802; the National Program on Global Change and Air-Sea Interaction, Grant/Award Numbers: GASI-IPOVAI-03, GASI-IPOVAI-06

Abstract

The Madden–Julian Oscillation (MJO) is characterized by slowly eastward-propagating precipitation and circulation anomalies with time scales of about 30–80 days. Both the phase and amplitude of the MJO fluctuate with time as it propagates eastward. Despite recent progress in understanding the predictability limit of the MJO as a whole, little is known of the difference in the predictability limits of its amplitude and phase. This paper investigates these differences using the nonlinear local Lyapunov exponent approach, which provides an estimate of atmospheric predictability based on observational data. The predictability limit of the phase of the MJO is determined as ~32 days, which is higher than that of its amplitude (about 16 days). In state-of-the-art operational forecast models, the phase of the MJO is also found to have a much better forecast skill than does its amplitude. The relatively low limit of the predictability of the amplitude will pose a challenge to MJO prediction.

KEYWORDS

amplitude, Madden–Julian oscillation (MJO), phase, predictability, the nonlinear local Lyapunov exponent (NLLE)

1 | INTRODUCTION

The Madden–Julian Oscillation (MJO) is the dominant component of intraseasonal (30–90 days) variability in the tropical atmosphere (Madden and Julian, 1994). The MJO has been shown to exert a large impact on many tropical weather and climate systems. For example, it can influence the variability of rainfall of the monsoon regions of Asia (Lau and Chan, 1986; Lawrence and Webster, 2002), Australia (Hendon and Liebmann, 1990), the west coast of North America (Mo and Higgins, 1998; Bond and Vecchi, 2003), and Africa (Matthews, 2004). It modulates the genesis of tropical cyclones in the Pacific Ocean and the Caribbean (Liebmann *et al.*, 1994; Nieto Ferreira *et al.*, 1996; Maloney and Hartmann, 2000; Hall *et al.*, 2001; Higgins and Shi, 2001), and affects equatorial surface winds in the Atlantic Ocean (Foltz and McPhaden, 2004). It also influences the variability and predictability of extratropical circulation (Ferranti *et al.*, 1990; Higgins and Mo, 1997; Jones *et al.*, 2004). Given the

importance of the MJO in its effects on the tropical and extratropical weather and climate systems, the predictability of the MJO is of particular interest as it could be used as a guide for future improvements in MJO prediction.

Numerous studies have examined the predictability limit or the forecast skill of tropical intraseasonal variability. For example, Reichler and Roads (2005) demonstrated that the useful forecast skill of the MJO for a perfect model and perfect initial and boundary conditions is about 4 weeks. Neena *et al.* (2014) reported that the predictability of the MJO in most of the models ranges from 20 to 45 days. In addition, several recent studies have demonstrated that the useful predictive skill of the MJO can reach 5 weeks (Vitart, 2017; Kim *et al.*, 2018; Lim *et al.*, 2018). These studies are mainly based on numerical models, and their results may be model-dependent. In recent years, the predictability of the MJO obtained by some nonlinear approaches is comparable with the skill demonstrated by dynamical multimodel ensembles (Kondrashov *et al.*, 2013; Zhang *et al.*, 2013; Chen *et al.*, 2014). Ding *et al.* (2010) employed a new approach called the nonlinear local Lyapunov exponent (NLLE) to investigate the predictability of the MJO using observational data, and they found the predictability limit of the MJO to be ~5 weeks, which is close to the useful forecast skill of the MJO derived from current operational forecasting systems.

The studies mentioned above focus on the predictability limit of the MJO as a whole. Given that both the amplitude and phase of the MJO are time-varying as the MJO propagates (Straub, 2013), it is quite possible that the predictability limits of the amplitude and phase of the MJO are different. However, to date, little is known of the difference in their predictability limits. In the present study, we focus our efforts on investigating the difference in the predictability limits of the amplitude and phase of the MJO by applying the NLLE method to observational data.

2 | DATA AND METHODOLOGY

2.1 | Observational and forecast data

We use the observed daily outgoing longwave radiation (OLR) data from the National Oceanic and Atmospheric Administration (NOAA). Because continuous OLR records are available from January 1, 1979 to the present, we use the continuous 1979–2017 time series in the global tropical strip (25°S–25°N). To corroborate results obtained from the OLR data, a similar record of daily 850-hPa and 200-hPa winds from the National Centers for Environmental Prediction–National Center for Atmospheric Research reanalysis (Kalnay *et al.*, 1996) is also employed. Additionally, the top net thermal radiation data (equal to the negative of OLR), 850-hpa zonal wind data and 200-hpa winds data with same record from the ECMWF (European Centre for Medium-Range Weather Forecasts) Interim Reanalysis (ERA-Interim) (Dee *et al.*, 2011) is used for this analysis to ensure that conclusions are independent on different dataset. All these data are analyzed on a 2.5° × 2.5° latitude–longitude grid.

For the purpose of real-time monitoring and prediction of the MJO (Wheeler and Hendon, Wheeler and Hendon, 2004) introduced the real-time multivariate MJO (RMM) index without time filtering. We also use the operational forecasts of the RMM index from the National Climate Center, China Meteorological Administration (NCC/CMA) to further explore the results of the operational forecasts of the MJO. The forecast RMM index is obtained from the Atmospheric General Circulation Model (AGCM2.2) developed at the NCC/CMA. The AGCM2.2 is a second-generation global spectral model, which has good simulation and forecasting capabilities for the MJO (Zhao et al., 2014; Zhao *et al.*, 2015; Wu *et al.*, 2016; Fang *et al.*, 2017). We analyzed forecast RMM index data from the NCC/CMA AGCM2.2 for four extended boreal winter [November–March (NDJFM)] (2015–2018).

2.2 | NLLE method

In the present study, the NLLE method is used to separately investigate the predictability limits of the amplitude and phase of the MJO. The NLLE is a nonlinear extension of the traditional Lyapunov exponent concept (Ding and Li, 2007). It can be employed to quantitatively estimate the predictability limit of various atmospheric and oceanic variables at different timescales by examining the evolution of the distance between initially local dynamical analogs (LDAs) from the observational time series (Ding and Li, 2011). Because the observational data contain a large proportion of the real information regarding the structure and propagation characteristics of the MJO, the NLLE method may provide a realistic estimate of the MJO predictability that does not depend on models (Ding *et al.*, 2010; Ding and Li, 2011). For a more detailed introduction to the NLLE method, please see the Supporting Information.

2.3 | Estimating the predictability limit of the MJO

To obtain the intraseasonal signal, the seasonal cycle of daily OLR, 850-hPa winds and 200-hPa velocity potential

derived from 200-hPa winds is first removed by subtracting the time mean and the first three harmonics of the annual cycle, leaving the anomaly field, which is then bandpass filtered to retain periods in the range 30–80 days. To extract the dominant MJO signal from the extended boreal winter (November–March; NDJFM) over the tropics (25°S–25°N), an empirical orthogonal function (EOF) analysis is performed on the bandpass-filtered OLR, 850-hPa winds and 200-hPa velocity potential.

The spatial structures of the leading two EOFs (EOF1 and EOF2) of the bandpass-filtered OLR, 850-hPa u-wind and 200-hPa velocity potential provide a good indication of large-scale MJO convection and circulation characteristics. The PC time series (PC1 and PC2) associated with EOF1 and EOF2 show the time-varying amplitude of the EOF spatial structures. Following Ding *et al.* (2010) and Ding and Li (2011), the MJO activity can be represented by the vector **Z** in the two-dimensional phase space defined by PC1 and PC2:

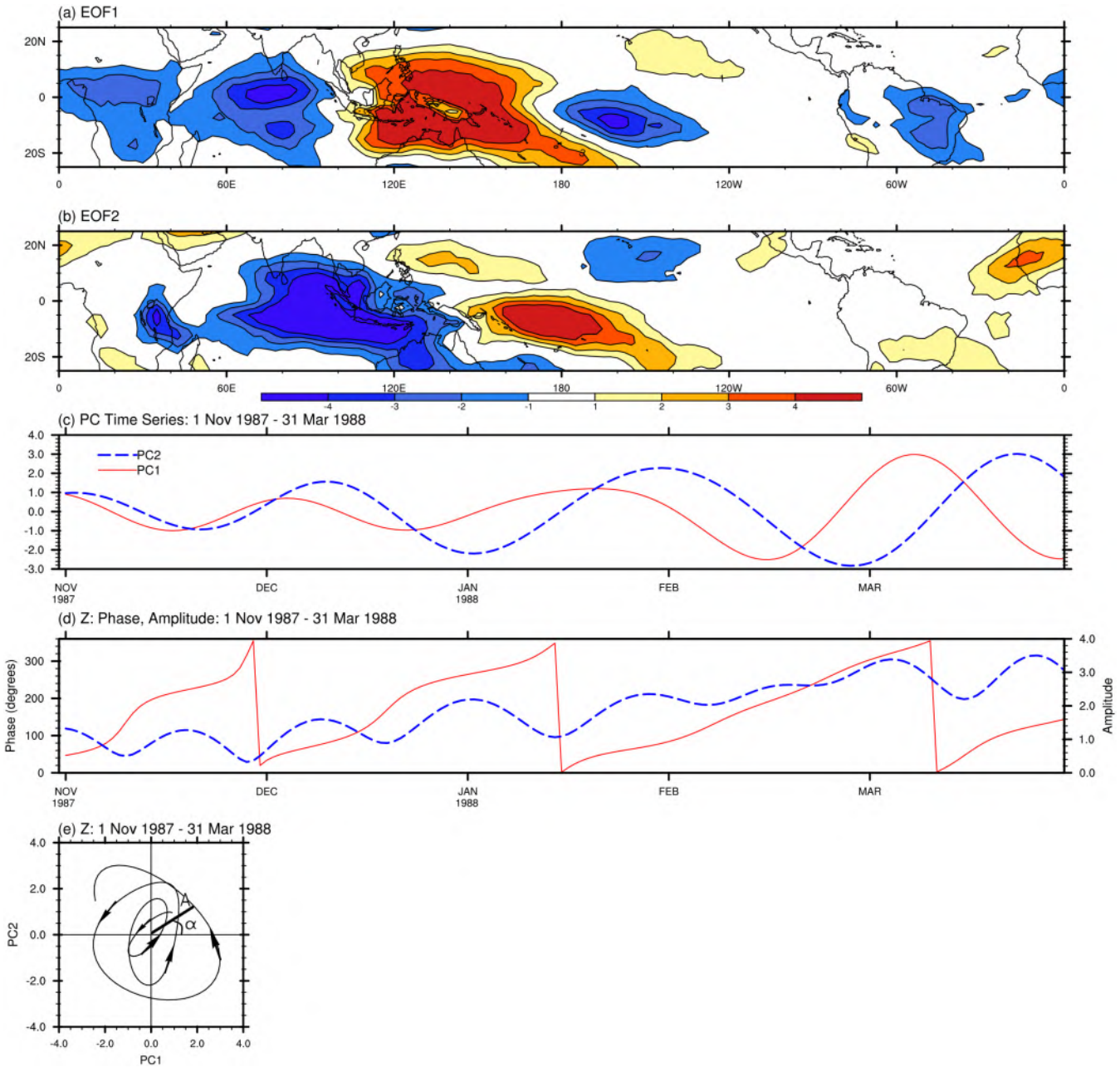

FIGURE 1 EOF analysis of 30–80-day-filtered OLR (W m^{-2}) during the extended winter (NDJFM) over the tropics (25°S–25°N). (a) EOF1, (b) EOF2. (c) PC1 (solid red line) and PC2 (dotted blue line) from October 1, 1987 to February 29, 1988. (d) Phase (solid red line; scale on left-hand axis) and amplitude (dotted blue line; scale on right-hand axis) of the vector **Z** from October 1, 1987 to February 29, 1988. (e) **Z** plotted from November 1, 1987 to March 31, 1988 in phase space

$$\mathbf{Z}(t) = \{PC1(t), PC2(t)\} \quad (1)$$

The eastward propagation of the MJO manifests itself as an anticlockwise rotation of the vector **Z** with time about the origin in phase space (Matthews, 2000). The mean error growth of the vector **Z** with time can be obtained using the NLLE approach. Once the error growth reaches the saturation level, almost all information on the initial states is lost and the prediction becomes meaningless. Therefore, the predictability limit can be quantitatively determined according to the saturation value of the error. To reduce the effects of sampling fluctuations, the predictability limit here is defined as the time at which the error reaches 95% of its saturation level.

To investigate the difference in the predictability limits of the amplitude and phase of the MJO, the time series of the amplitude A and phase α can be derived from PC1 and PC2 (Matthews, 2000):

$$A(t) = \left\{\mathrm{PC1}^2(t) + \mathrm{PC2}^2(t)\right\}^{1/2} \quad (2)$$

$$\alpha(t) = \tan^{-1}\{\mathrm{PC2}(t)/\mathrm{PC1}(t)\} \quad (3)$$

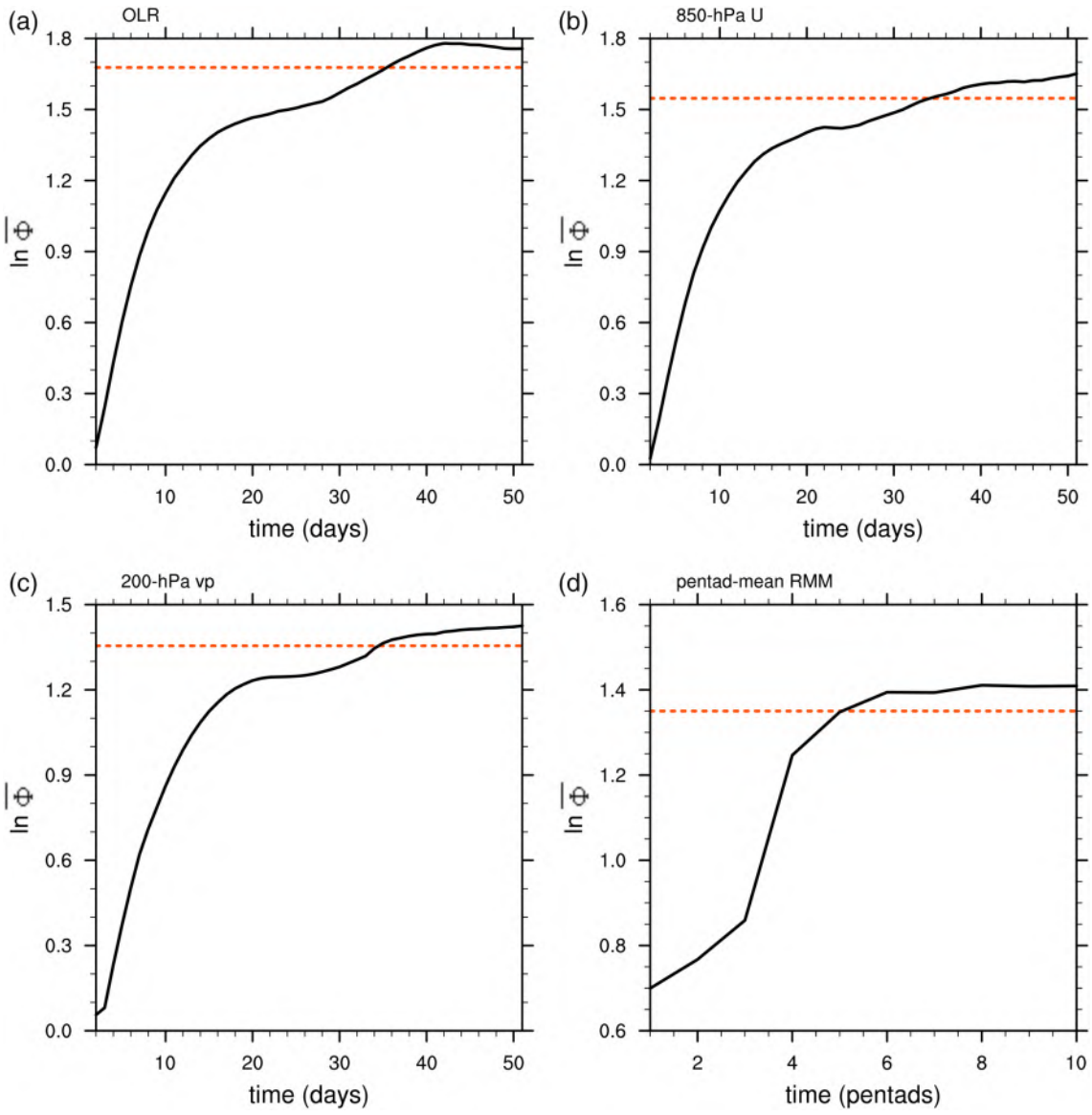

FIGURE 2 (a) Mean error growth of the vector **Z** in the two-dimensional phase space defined by the first two PCs of the filtered OLR during the extended winter (NDJFM), where **Z** represents the MJO activity. (b) As in (a), but the vector **Z** is defined with respect to the filtered 850-hPa zonal wind. (c) as in (a), but the vector **Z** is defined with respect to the filtered 200-hPa velocity potential. (d) As in (a), but the vector **Z** is defined by the pentad-mean RMM data. The dashed line represents the 95% level of the saturation value, as obtained by taking the average of the mean error growth after 50 days. The $\bar{\Theta}$ denotes the mean error of the vector

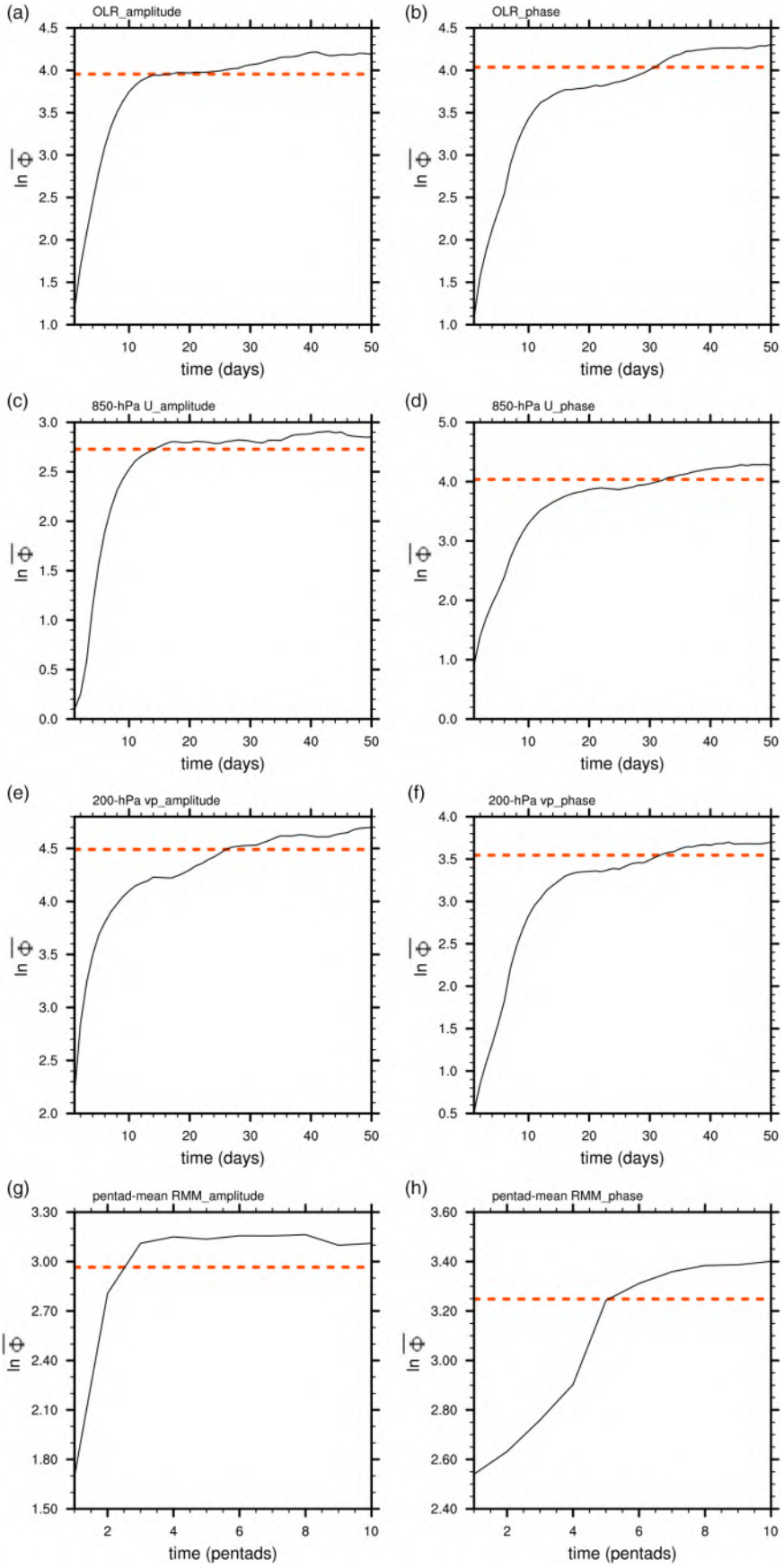

FIGURE 3 As in Figure 2, but the amplitude (left panels) and phase (right panels) of the MJO, as represented by **Z**, are shown separately. **Z** is defined in (a, b) by OLR, (c, d) by 850-hPa zonal wind, (e, f) by 200-hPa velocity potential, and (g, h) by RMM index

Based on the time series of A and α, we quantitatively determine the predictability limits of the amplitude and phase of the MJO using the NLLE method.

3 | RESULTS

The spatial structures of EOF1 and EOF2 of the filtered OLR are shown in Figure 1a,b, respectively. EOF1 is spatially in quadrature with EOF2, and together they describe the large-scale propagating convective anomalies associated with the MJO. The PC time series associated with EOF1 and EOF2 are shown in Figure 1c, characterized by PC1 leading PC2 by about a quarter cycle. These features are consistent with the eastward propagation of the MJO.

Using the NLLE method, we compute the mean error growth of the vector **Z**, which consists of PC1 and PC2. We note that the mean error of **Z** initially increases quickly, then slows down, and finally reaches saturation (Figure 2a). Ding *et al*. (2010) pointed out that in the initial 2 weeks, the initial conditions may play an important role in determining the initial error growth of the MJO, but after ~2 weeks the error growth may be more strongly influenced by the slowly varying boundary conditions, such as the sea surface temperature (SST). From Figure 2a, the predictability limit of the MJO determined from the filtered OLR data is ~35 days. These results are generally consistent with Ding *et al*. (2010) and Ding and Li (2011).

Based on Equations (2) and (3), the time series of A and α of the MJO can be obtained from PC1 and PC2. It is evident that the amplitude A fluctuates more rapidly than the phase α (Figure 1d). The eastward propagation of the MJO is generally associated with an increase in the phase α and an irregular fluctuation of the amplitude A with time (Figure 1e). By applying the NLLE method to the time series of A and α, we can obtain their mean error growth curves (Figure 3a,b). We note that the mean errors of both the amplitude A and phase α initially increase quickly over 2 weeks. Subsequently, the error of A quickly reaches saturation, whereas α experiences a slow growth before saturation. According to the 95% threshold of the error saturation level, we determined the predictability limits of the amplitude A and phase α of the MJO to be around 16 and 32 days, respectively. This predictability limit of the phase α is higher than that of the amplitude A, and is close to the predictability limit of the MJO itself.

We further used the filtered 850-hPa zonal wind and 200-hPa velocity potential to compare the predictability limits of the amplitude A and phase α of the MJO. We performed EOF analysis of the filtered 850-hPa zonal wind or 200-hPa velocity potential over the tropics (25°S–25°N) in the same way to extract the large-scale circulation characteristics associated with the MJO

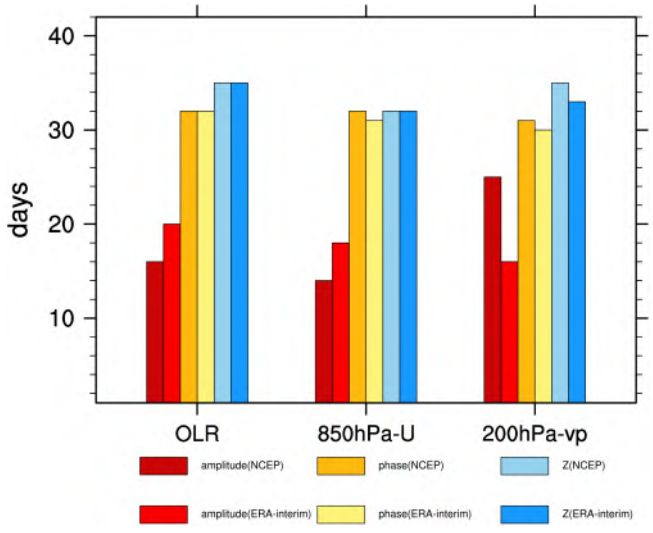

FIGURE 4 The predictability limits of the vector **Z** together with its amplitude and phase based on two different reanalysis datasets (from NCEP and ERA-interim). Three kinds of bandpass-filtered variables are analyzed; from left to right: outgoing longwave radiation (or top net thermal radiation), 850-hPa zonal wind, and 200-hPa velocity potential

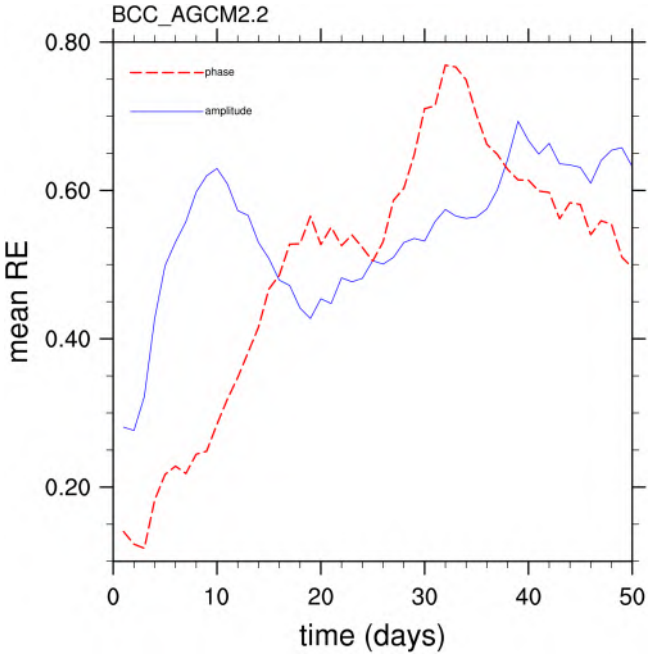

FIGURE 5 Mean relative errors (RE) of the MJO amplitude (solid blue line) and phase (dotted red line) based on data from the atmospheric general circulation model of NCC (BCC_AGCM2.2)

(not shown). The PC time series associated with EOF1 and EOF2 of the filtered 850-hPa zonal wind and 200-hPa velocity potential can be obtained. Then the time series of A and α of the MJO can be derived from these PC time series based on Equations (2) and (3). As for the OLR, the amplitude A fluctuates more rapidly than the phase α for both the 850-hPa zonal wind and 200-hPa velocity potential.

The mean error growth curves of the MJO, its amplitude A and phase α for the 850-hPa zonal wind and 200-hPa velocity potential are shown in Figures 2 and 3, respectively. The error curves of the 850-hPa zonal wind and 200-hPa velocity potential have similar characteristics to those of the OLR. The predictability limits of the MJO determined from the 850-hPa zonal wind and 200-hPa velocity potential are close (~35 days). The predictability limits of the phase α determined from the 850-hPa zonal wind and 200-hPa velocity potential are 32 and 31 days, respectively, both of which are higher than the limits of the amplitude A (14 and 25 days, respectively).

The predictability limits of the MJO as well as its amplitude A and phase α presented above are derived from bandpass-filtered variables. The use of temporal filtering tends to overestimate the predictability of the MJO because this filtering includes future information (Ding *et al.*, 2010). It is therefore interesting to examine the predictability limits of the amplitude and phase of the

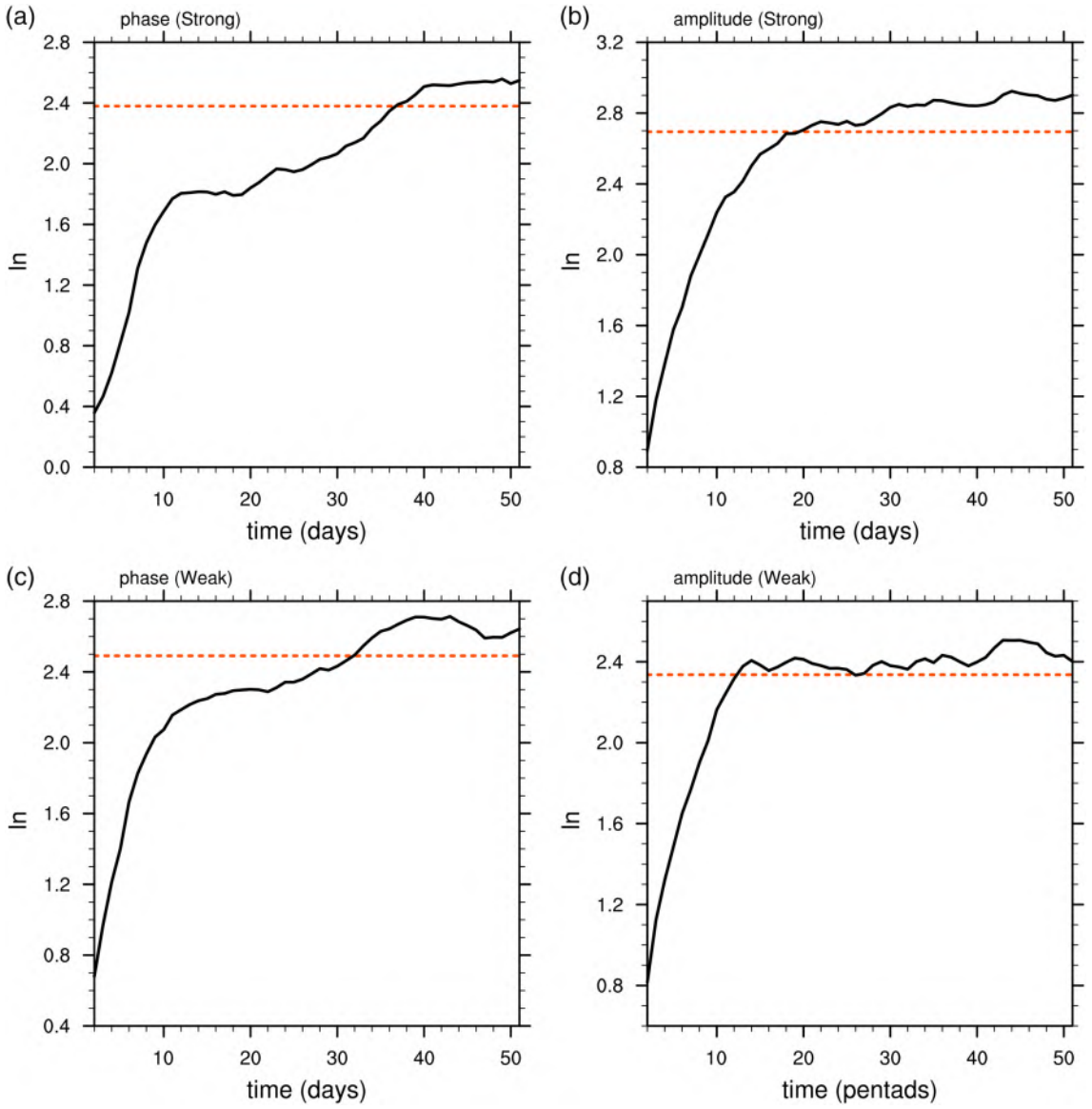

FIGURE 6 Mean error growth of the phase (left panels) and amplitude (right panels) of the strong MJO event (up panels) and weak MJO event (down panels). Strong MJO events were defined as those with amplitude greater than or equal to 1.0, and weak MJO events were defined as those with amplitude less than 1.0

MJO using the RMM indices that do not employ temporal filtering. The predictability limit of the MJO based on the pentad RMM indices is ~25 days (Figure 2d), which is lower than the predictability limit of ~5 weeks based on bandpass-filtered variables obtained above. This difference may reflect the influence of temporal filtering on the predictability of the MJO (Ding *et al.*, 2010). For RMM indices, the phase of the MJO still shows a higher predictability limit than does its amplitude (25 days versus 12 days) (Figure 3g,h), consistent with the predictability obtained from bandpass-filtered OLR, the 850-hPa zonal wind, or the 200-hPa velocity potential.

The predictability limits of the MJO as well as its amplitude A and phase α determined from different variables and different reanalysis datasets are summarized in Figure 4. Regardless of the variables and reanalysis datasets used, the predictability limit of the phase of the MJO is higher than that of its amplitude. This suggests that the amplitude of the MJO is less predictable than its phase. The relatively low limit of the predictability of the amplitude will pose a challenge for MJO prediction. In addition, we note that the predictability limit of the phase of the MJO is close to that of the MJO itself, indicating that the predictability of the MJO may mainly arise from that of its phase.

The results presented above compare the predictability limits of the amplitude and phase of the MJO based on observational data. The question naturally arises as to whether the forecast skill of the phase of the MJO is

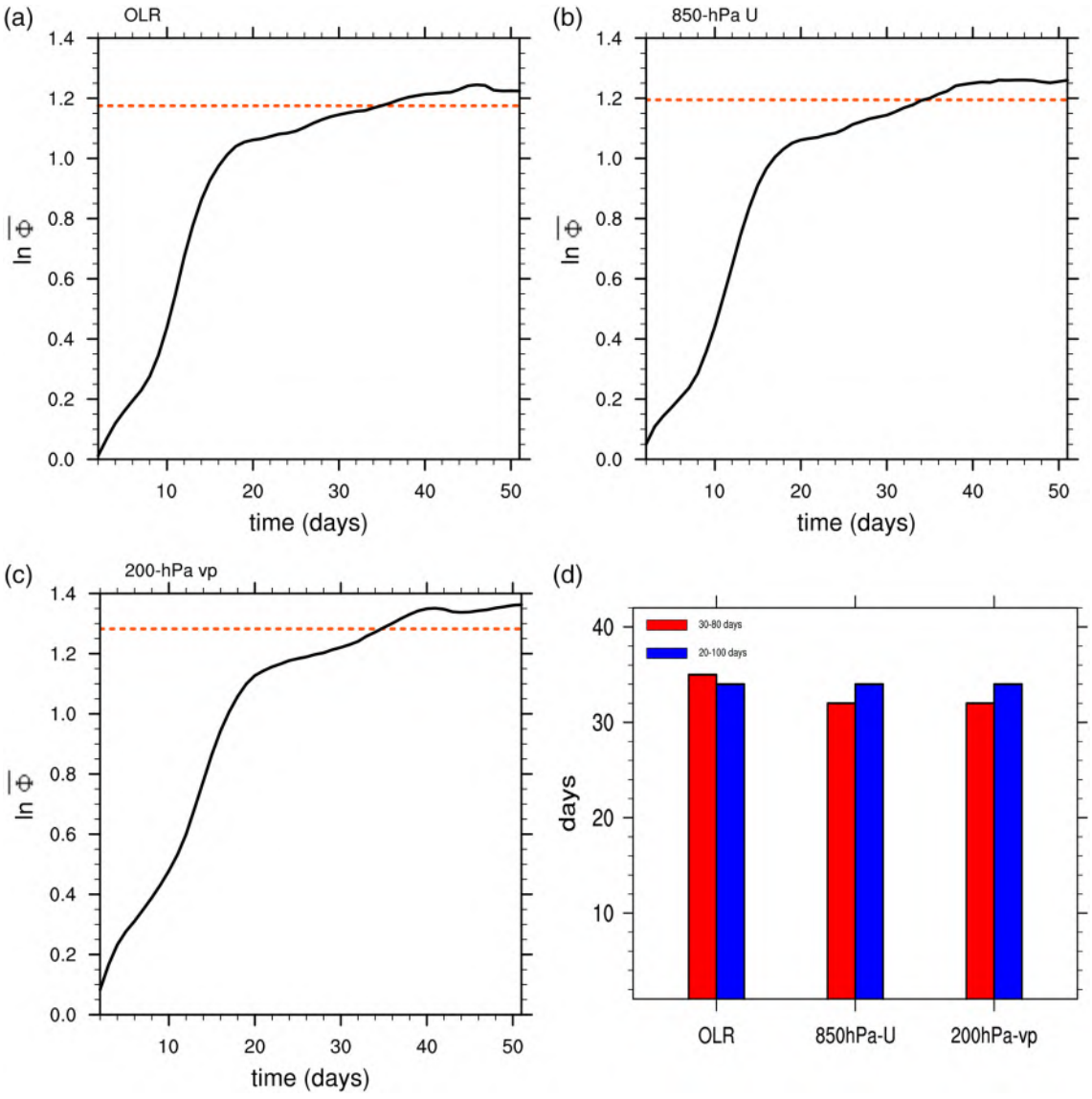

FIGURE 7 Mean error growth of the vector **Z** based on different bandpass-filtered (20–100 days) variables: (a) outgoing longwave radiation, (b) 850-hPa zonal wind, and (c) 200-hPa velocity potential. (d) The predictability limits of the vector **Z** calculated from bandpass filtering in two different bands: 30–80 days (red bar) and 20–100 days (blue bar)

higher than that of its amplitude in current operational forecasts. The MJO operational forecasts for the most recent four-extended-winter (2015–2018) from the NCC/CMA were analyzed (as in Figure 5). Results indicate that the error of the phase shows slower growth than that of the amplitude. The amplitude error reaches the first peak ~10 days, whereas the phase error does not reach the peak until 20 days later. These results suggest that the phase has a much better forecast skill than the amplitude in state-of-the-art operational forecasts of the MJO, consistent with the observational results. In addition, we note that the forecast skills of both the MJO phase and amplitude in the operational forecast models from the NCC/CMA are below their predictability limits. This implies that a significant increase in the forecast skill of the MJO amplitude and phase may be achievable through model improvements. These results may be a useful guide for the improvement of forecast models.

4 | CONCLUSIONS AND DISCUSSION

Using the NLLE method, this study investigated differences in the predictability limits of the amplitude and phase of the MJO derived from the observed bandpass-filtered (30–80 days) OLR, 850-hPa u-wind, and 200-hPa velocity potential. Two different reanalysis date sets were used in this study: the NCEP and ERA-Interim. Similar results were obtained for these different variables and different reanalysis datasets. The predictability limit of the phase of the MJO is ~32 days, close to that of the MJO itself but higher than the predictability limit of the amplitude of the MJO (~16 days). The relatively low predictability limit of the amplitude may arise from the rapid fluctuation of the amplitude itself. In contrast, the phase of the MJO fluctuates more slowly, possibly leading to a higher predictability limit. Our investigation of the MJO operational forecasts from the NCC/CMA has revealed that the phase has a much better forecast skill than the amplitude. The limited forecast skill for amplitude in state-of-the-art operational forecast models will pose a challenge for MJO prediction.

The above findings lead us to conclude that the predictability limit of the phase of the MJO is higher than that of its amplitude. However, considering that the predictability of strong and weak MJO events are quite different (Neena *et al*., 2014; Kim *et al*., 2018), we also analyzed the predictability limits of the amplitude and phase of the MJO for strong and weak MJO events, respectively (Figure 6). The result shows that the predictability limit of the phase is higher than that of the amplitude for both strong and weak MJO events. In addition, considering that bandpass filtering with different bands could affect the predictability estimate (Ding *et al*., 2016), we also performed a similar analysis by applying the 20–100 days bandpass filtering instead of by applying the 30–80 days filtering (Figure 7). We found that the difference of the predictability limit of the MJO between two different bands is small by using NLLE approach. This result suggests that our conclusion is not sensitive to the choice of the bandpass filtering.

ACKNOWLEDGEMENTS

This work was jointly supported by the National Key Research and Development Project (2018YFC1505802), and the National Program on Global Change and Air-Sea Interaction (GASI-IPOVAI-03, GASI-IPOVAI-06).

ORCID

Deyu Lu https://orcid.org/0000-0001-8322-5296

REFERENCES

Bond, N.A. and Vecchi, G.A. (2003) The influence of the Madden–Julian oscillation on precipitation in Oregon and Washington. *Weather Forecasting*, 18, 600–613.

Chen, N., Majda, A.J. and Giannakis, D. (2014) Predicting the cloud patterns of the Madden-Julian oscillation through a low-order nonlinear stochastic model. *Geophysical Research Letters*, 41, 5612–5619. https://doi.org/10.1002/2014GL060876.

Dee, D.P., Uppala, S.M., Simmons, A.J., Berrisford, P., Poli, P., Kobayashi, S., Andrae, U., Balmaseda, M.A., Balsamo, G., Bauer, P., Bechtold, P., Beljaars, A.C.M., van de Berg, L., Bidlot, J., Bormann, N., Delsol, C., Dragani, R., Fuentes, M., Geer, A.J., Haimberger, L., Healy, S.B., Hersbach, H., Hólm, E. V., Isaksen, L., Kållberg, P., Köhler, M., Matricardi, M., McNally, A.P., Monge-Sanz, B.M., Morcrette, J.J., Park, B.K., Peubey, C., de Rosnay, P., Tavolato, C., Thépaut, J.N. and Vitart, F. (2011) The ERA-interim reanalysis: configuration and performance of the data assimilation system. *Quarterly Journal of the Royal Meteorological Society*, 137, 553–597.

Ding, R.Q. and Li, J.P. (2007) Nonlinear finite-time Lyapunov exponent and predictability. *Physics Letters*, 364A, 396–400.

Ding, R.Q. and Li, J.P. (2011) Estimate of the predictability of boreal summer and winter intraseasonal oscillations from observations. *Monthly Weather Review*, 139, 2421–2438. https://doi.org/10.1175/2011MWR3571.1.

Ding, R.Q., Li, J.P. and Seo, K.-H. (2010) Predictability of the Madden–Julian oscillation estimated using observational data. *Monthly Weather Review*, 138, 1004–1013.

Ding, R.Q., Li, J.P., Zheng, F., Feng, J. and Liu, D.Q. (2016) Estimating the limit of decadal-scale climate predictability using observational data. *Climate Dynamics*, 46, 1563–1580. https://doi.org/10.1007/s00382-015-2662-6.

Fang, Y.J., Wu, P.L., Wu, T.W., Wang, Z.Z., Zhang, L., Liu, X.W., Xin, X.G. and Huang, A.N. (2017) An evaluation of boreal summer intra-seasonal oscillation simulated by BCC_AGCM2.2. *Climate Dynamics*, 48(9–10), 3409–3423. https://doi.org/10.1007/s00382-016-3275-4.

Ferranti, L., Palmer, T.N., Molteni, F. and Klinker, K. (1990) Tropical-extratropical interaction associated with the 30–60 day oscillation and its impact on medium and extended range prediction. *Journal of the Atmospheric Sciences*, 47, 2177–2199.

Ferreira, R.N., Schubert, W.H. and Hack, J.J. (1996) Dynamical aspects of twin tropical cyclones associated with the Madden–Julian oscillation. *Journal of the Atmospheric Sciences*, 53, 929–945.

Foltz, G.R. and McPhaden, M.J. (2004) The 30–70 day oscillations in the tropical Atlantic. *Geophysical Research Letters*, 31, L15205. https://doi.org/10.1029/2004GL020023.

Hall, J.D., Matthews, A.J. and Karoly, D.J. (2001) The modulation of tropical cyclone activity in the Australian region by the Madden–Julian oscillation. *Monthly Weather Review*, 129, 2970–2982.

Hendon, H.H. and Liebmann, B. (1990) The intraseasonal (30–50 day) oscillation of the Australian summer monsoon. *Journal of the Atmospheric Sciences*, 47, 2909–2923.

Higgins, R.W. and Mo, K.C. (1997) Persistent North Pacific circulation anomalies and the tropical intraseasonal oscillation. *Journal of the Atmospheric Sciences*, 10, 223–244.

Higgins, R.W. and Shi, W. (2001) Intercomparison of the principal modes of interannual and intraseasonal variability of the North American monsoon system. *Journal of Climate*, 14, 403–417.

Jones, C., Waliser, D.E., Lau, K.M. and Stern, W. (2004) The Madden–Julian oscillation and its impact on Northern Hemisphere weather predictability. *Monthly Weather Review*, 132, 1462–1471.

Kalnay, E., Kanamitsuand, M., Kistler, R. and Collins, W.G. (1996) The NCEP/NCAR 40-year reanalysis project. *Bulletin of the American Meteorological Society*, 77, 437–471.

Kim, H., Vitart, F. and Waliser, D.E. (2018) Prediction of the Madden–Julian oscillation: a review. *Journal of Climate*, 31, 9425–9433.

Kondrashov, D., Chekroun, M.D., Robertson, A.W. and Ghil, M. (2013) Low-order stochastic model and past-noise forecasting of the Madden-Julian oscillation. *Geophysical Research Letters*, 40, 5305–5310. https://doi.org/10.1002/grl.50991.

Lau, K.-M. and Chan, P.H. (1986) Aspects of the 40–50 day oscillation during the northern summer as inferred from outgoing longwave radiation. *Monthly Weather Review*, 114, 1354–1367.

Lawrence, D.M. and Webster, P.J. (2002) The boreal summer intraseasonal oscillation: relationship between northward and eastward movement of convection. *Journal of the Atmospheric Sciences*, 59, 1593–1606.

Liebmann, B., Hendon, H. and Glick, J. (1994) The relationship between tropical cyclones of the western Pacific and Indian oceans and the Madden–Julian oscillation. *Journal of the Meteorological Society of Japan*, 72, 401–411.

Lim, Y., Son, S.-W. and Kim, D. (2018) MJO prediction skill of the subseasonal-to-seasonal prediction models. *Journal of Climate*, 31, 4075–4094. https://doi.org/10.1175/JCLI-D-17-0545.1.

Madden, R.A. and Julian, P.R. (1994) Observations of the 40–50-day tropical oscillation—a review. *Monthly Weather Review*, 122, 814–837.

Maloney, E.D. and Hartmann, D.L. (2000) Modulation of eastern North Pacific hurricanes by the Madden–Julian oscillation. *Journal of Climate*, 13, 1451–1460.

Matthews, A.J. (2000) Propagation mechanisms for the Madden–Julian oscillation. *Quarterly Journal of the Royal Meteorological Society*, 126, 2637–2651. https://doi.org/10.1002/qj.49712656902.

Matthews, A.J. (2004) Intraseasonal variability over tropical Africa during northern summer. *Journal of Climate*, 17, 2427–2440.

Mo, K. and Higgins, R.W. (1998) Tropical convection and precipitation regimes in the western United States. *Journal of Climate*, 10, 3028–3046.

Neena, J.M., Lee, J.Y., Waliser, D., Wang, B. and Jiang, X. (2014) Predictability of the Madden–Julian oscillation in the intraseasonal variability hindcast experiment (ISVHE). *Journal of Climate*, 27, 4531–4543.

Reichler, T. and Roads, J.O. (2005) Long-range predictability in the tropics. Part II: 30–60-day variability. *Journal of Climate*, 18, 634–650.

Straub, K.H. (2013) MJO initiation in the real-time multivariate MJO index. *Journal of Climate*, 26(4), 1130–1151. https://doi.org/10.1175/JCLI-D-12-0074.1.

Vitart, F. (2017) Madden–Julian oscillation prediction and teleconnections in the S2S database. *Quarterly Journal of the Royal Meteorological Society*, 143, 2210–2220. https://doi.org/10.1002/qj.3079.

Wheeler, M.C. and Hendon, H.H. (2004) An all-season real-time multivariate MJO index: development of an index for monitoring and prediction. *Monthly Weather Review*, 132, 1917–1932. https://doi.org/10.1175/1520-0493(2004)1322.0.CO;2.

Wu, J., Ren, H.L., Zuo, J.Q., Zhao, C.B., Chen, L.J. and Li, Q.P. (2016) MJO prediction skill, predictability, and teleconnection impacts in the Beijing Climate Center Atmospheric General Circulation Model. *Dynamics of Atmospheres and Oceans*, 75, 78–90. https://doi.org/10.1016/j.dynatmoce.2016.06.001.

Zhang, C., Gottschalck, J., Maloney, E.D., Moncrieff, M.W., Vitart, F., Waliser, D.E., Wang, B. and Wheeler, M.C. (2013) Cracking the MJO nut. *Geophysical Research Letters*, 40, 1223–1230. https://doi.org/10.1002/grl.50244.

Zhao, C.B., Ren, H.L., Song, L.C. and Wu, J. (2015) Madden–Julian oscillation simulated in BCC climate models. *Dynamics of Atmospheres and Oceans*, 72, 88–101. https://doi.org/10.1016/j.dynatmoce.2015.10.004.

Zhao S.Y., Zhi X.F., Zhang H., Wang Z.L. and Wang Z.Z. (2014) Primary Assessment of the Simulated Climatic State Using a Coupled Aerosol-Climate ModelBCC_AGCM2.0.1_CAM. *Climatic and Environmental Research*, 19, 265-277 (in Chinese). https://doio.org/10.3878/j.issn.1006-9585.2012.12015.

SUPPORTING INFORMATION

Additional supporting information may be found online in the Supporting Information section at the end of this article.

How to cite this article: Lu D, Ding R, Li J. The predictability limit of the amplitude and phase of the Madden-Julian oscillation. *Atmos Sci Lett*. 2020;21:e968. https://doi.org/10.1002/asl.968